HHS Public Access

Author manuscript

*JACC Basic Transl Sci*. Author manuscript; available in PMC 2017 August 08.

Published in final edited form as:

*JACC Basic Transl Sci*. 2017 June ; 2(3): 258–269. doi:10.1016/j.jacbts.2017.02.002.

# Increased afterload following myocardial infarction promotes conduction-dependent arrhythmias that are unmasked by hypokalemia

**Lukas J. Motloch, MD, PhD**, **Kiyotake Ishikawa, MD**, **Chaoqin Xie, MD**, **Jun Hu, PhD**, **Jaume Aguero, MD**, **Kenneth M. Fish, PhD**, **Roger J. Hajjar, MD**, and **Fadi G. Akar, PhD, FHRS**

Cardiovascular Institute, Icahn School of Medicine at Mount Sinai, New York, NY, USA

## SUMMARY

Although the pathophysiological significance of resistant hypertension in post-myocardial infarction (MI) patients is established, mechanisms by which increased afterload in that setting worsens outcome are unclear. With regards to sudden cardiac death, whether increased afterload alters the electrophysiological substrate following MI is unknown. We established a new large animal model of chronic post-MI remodeling with increased afterload which exhibits widespread deposition of fibrosis in remote areas from the anterior MI, mimicking the disease phenotype of patients with advanced ischemic heart disease. We identified the mode-of-initiation and mechanism of arrhythmias which were consistently unmasked by hypokalemia in this clinically-relevant model.

### Keywords

Hypokalemia; Myocardial infarction; Increased Afterload; Arrhythmias; Conduction

## Introduction

Hypertension confers the greatest risk of cardiovascular-related mortality and morbidity. Despite major improvements in pharmacotherapies, the prevalence of hypertension in patients with coronary artery disease who are predisposed to myocardial infarction (MI) and sudden cardiac death (SCD), remains unacceptably high (1). Although the pathophysiological significance of hypertension in post-MI patients is well established, mechanisms by which increased afterload in that setting exacerbates injury and worsens outcome are unclear. With regards to SCD, whether and how increased afterload alters the electrophysiological substrate and promotes arrhythmias following MI is unknown. We

Corresponding Author: Fadi G. Akar, PhD, FHRS, Cardiovascular Research Center, Icahn School of Medicine at Mount Sinai, One Gustave L. Levy Place, Box 1030, New York, NY 10029-6574 USA, Phone: +1-212-824-8920; Fax: +1-212-241-4080; fadi.akar@mssm.edu.

**Disclosures:** All authors declare no conflict of interests.

established a new large animal model of chronic post-MI remodeling with increased afterload (MI/iAL) which exhibits widespread deposition of fibrosis in remote areas from the anterior MI, mimicking the disease phenotype of patients with advanced ischemic heart disease. The abundant presence of diffuse fibrosis across the left ventricle (LV) in MI/iAL pigs led us to hypothesize that chronically increased afterloads in the setting of post-MI remodeling create a substrate for ventricular arrhythmias. To address this hypothesis, we performed a systematic evaluation of the electrophysiological substrate using high-resolution optical action potential mapping in arterially-perfused wedge preparations before and after challenge with hypokalemia, an ionic stressor that has been shown to exert a preferential pro-arrhythmic effect in fibrotic aged hearts (2). Post-MI pigs with increased afterload (MI/iAL) were compared to those that underwent standard MI induction without increased afterload and to naïve control animals (Ctrl). We identified the mode-of-initiation and mechanism of arrhythmias which were consistently unmasked by hypokalemia in this clinically-relevant large animal model of MI/iAL.

## Methods

### Experimental protocols

All animal handling and care complied with the NIH Guide for the Care and Use of Laboratory Animals. All protocols were approved by the Institutional Animal Care and Use Committee of the Icahn School of Medicine at Mount Sinai. Twenty five female Yorkshire pigs (~20 Kg) were included. Seventeen pigs were assigned to either the MI/iAL (N=9) or the MI groups (N=8). The Ctrl group consisted of eight pigs that neither underwent MI nor aortic banding. The MI/iAL and MI groups underwent MI induction on day 0. MI/iAL pigs underwent a secondary procedure of ascending aortic banding 1-month after MI. This time-point was chosen to evaluate the impact of increased afterload in the setting of chronic MI, which follows the phase of active healing. Echocardiography was performed at 1-month, 2-months, and 3-months after MI. Animals were subsequently euthanized and porcine wedge preparations were isolated and arterially-perfused *ex vivo* for optical action potential mapping studies (Figure 1) as described previously (3–7). Tissue specimens were collected for histological and molecular analyses, including assessment of fibrosis and fibrosis-related gene expression.

### Animal model of MI/iAL

Details of the MI induction procedure have been described with visual guidance (8). Details of the aortic banding procedure have also been reported by our group (9). In brief, isofluorane-based anesthesia was initiated. A left-sided thoracotomy was performed through the 3$^{rd}$ inter-costal space, and a small incision was created on the pericardium. The pulmonary artery was pulled gently and the ascending aorta was isolated and banded. The degree of stenosis was determined by evaluating the ratio of the velocity-time integral (VTI) at the LV outflow tract and the site of stenosis. We aimed for a VTI ratio of 0.25–0.35 based on our recent report (9). VTI ratios <0.25 are associated with a high rate of early mortality whereas those over 0.35 are associated with minor remodeling. Using this approach, we reported a 1.7X increase in fibrosis across the LV (9).

Comprehensive trans-thoracic echocardiographic studies including Doppler, two-dimensional, and three-dimensional echocardiography (2DE and 3DE, respectively) were performed. A Philips iE-33 ultrasound system (Philips Medical Systems, Andover, MA) was used to acquire echocardiographic data with a multi-frequency imaging transducer. LV volumes and ejection fractions (EF) were obtained from 3DE images.

### Transmural optical action potential mapping in porcine wedge preparations

We previously developed the technique of transmural optical action potential mapping in arterially perfused canine wedge preparations (3–5,7). The utility of this technique has been elegantly expanded by the Efimov group to wedges from explanted human hearts (10–15). Here, we applied the same procedure in the pig heart. Briefly, wedges of porcine myocardium (Figure 1A) were dissected from the mid apico-basal region adjacent to the anterior infarct, a region known to support post-MI arrhythmias. Wedges were arterially-perfused via a secondary branch of the high lateral or posterolateral LCx and optical mapping was performed using the voltage-sensitive dye, di-4-ANEPPS (Figure 1B), as previously reported in dogs (3–7). Porcine wedge preparations were isolated from Ctrl (N=8 pigs, n=12 wedges), MI (N=5 pigs, n=10 wedges) and MI/iAL (N=6 pigs, n=12 wedges) animals for detailed electrophysiological studies. A subset of 7 Ctrl, 8 MI, and 8 MI/iAL preparations was specifically used to test the effects of hypokalemia on electrophysiological properties and arrhythmia vulnerability. For these, preparations were paced at 1.5X the diastolic threshold over a wide range of pacing rates (1.0Hz – 6.0Hz in 0.5Hz increments with pacing at each rate lasting for at least 2 min before recordings were obtained) during perfusion with normal Tyrodes solution (normokalemia, $K^+$ 4mM) followed by low-$K^+$ solution (hypokalemia, $K^+$ 2mM).

We measured CV along the transmural axis of impulse propagation by averaging the magnitude of the velocity vectors along that direction. Basal CV ($CV_b$) was defined as CV during normokalemia at a PCL of 1000ms. The critical CV ($CV_c$) was defined as the CV that was recorded at the fastest pacing rate before onset of VT/VF, loss of 1:1 pacing capture, or the end of the experimental protocol (hypokalemia, 6.0Hz) if neither VT/VF nor loss-of-capture occurred. VT/VF was defined as pacing-induced tachyarrhythmias which were sustained for at least 2 minutes. The protocol was terminated upon VT/VF occurrence.

### Histology and molecular analyses

Formalin-fixed tissue blocks from the non-infarcted myocardium were embedded in paraffin, sectioned (8μm), mounted, and stained with wheat-germ agglutinin (WGA) labeled with fluorescein isothiocyanate (for assessing hypertrophy) or picro-sirius red (for assessing fibrosis). A subset of hearts was stained with triphenyl-tetrazolium chloride to highlight the scar area relative to viable tissue and the size of the scar was assessed by digital planimetry.

### RT-PCR

Total RNA was isolated using acid guanidinium thiocyanate-phenol-chloroform extraction by 1 ml TRIzol reagent (Life Technologies). Total RNA was reverse transcribed into first-strand cDNA using High-Capacity cDNA Reverse Transcription Kit with RNase inhibitor (Applied Biosystems) with random primers. Real-time PCR was performed using the 7500

Fast Real-Time PCR System and Fast SYBR® green PCR master mix (Applied Biosystems) in duplicate. High-resolution melting curves were generated to confirm the specificity of the PCR products. After rectification by the passive reference dye Rox within the master mix, the threshold cycle ($C_T$) values were determined using SDS version 1.5.1 (Applied Biosystems). The relative mRNA expression levels of a given gene were evaluated by the $2^{-\Delta CT}$ method. mRNA levels of each target gene were normalized to those of the internal control, GAPDH. Primers used in this study are shown below (Table 1):

### Statistical analysis

N and n refer to the numbers of pigs and arterially-perfused wedge preparations, respectively. Hemodynamic measurements (performed in animals) are expressed as mean ±SD. Electrophysiological measurements (performed in wedges) are expressed as mean ±SEM. Differences between groups were evaluated using Chi-square testing for discrete variables (presence vs absence of VT/VF, maintenance vs loss of 1:1 capture). For continuous variables, the Shapiro-Wilk test was applied to test for normal distribution of data for a given metric in a given group. If data was normally distributed Student-t test or analysis of variance (ANOVA) followed by Tukey's test were performed. The unpaired t-test was used to compare differences between two groups. For multiple comparisons, one-way ANOVA followed by post-hoc Tukey's test was calculated. If normal distribution could not be confirmed, Kruskal-Wallis or Mann-Whitney U were applied. $p<0.05$ was considered statistically significant. The total number of preparations used in each figure is indicated in the corresponding figure legend. Statistical analyses were performed using the SPSS v22 software.

## Results

Successful aortic banding in MI/iAL animals was confirmed by echocardiography as the VTI ratio was markedly decreased compared to MI animals that were not subjected to aortic banding (0.29±0.08 vs 0.73±0.11, $p<0.001$). Surprisingly, the extent of mechanical dysfunction in MI/iAL and MI animals was similar as both groups exhibited a comparable decrease in $dP/dt_{max}$ (MI/iAL: 1935±749 mmHg/sec, MI: 2111±661 mmHg/sec, Ctrl: 2855±814 mmHg/sec; ANOVA: $p=0.10$ with post hoc MI/iAL vs. MI: $p=0.65$) and an increase in LV end-diastolic pressure (MI/iAL: 20.7±5.8 mmHg, MI: 19.8±4.8 mmHg, Ctrl: 12.9±3.8 mmHg; ANOVA: $p=0.02$ with post hoc MI/iAL vs. MI: $p=0.75$) compared to their Ctrl counterparts.

Unlike mechanical function, structural remodeling was significantly more advanced in MI/iAL compared to MI animals despite a comparable scar size (Figure 1C). Picro-sirius red staining revealed increased (by ~2 fold) interstitial fibrosis in the MI/iAL compared to MI animals (Figure 1D & E). In addition, the expression of multiple pro-fibrotic genes and fibrosis markers including CTGF, TGF-β, Col1A1, and Col3A1 were markedly (1.5–3 fold, $p<0.01$) upregulated in MI/iAL compared to MI and Ctrl animals (Figure 1G). Cx43 mRNA expression exhibited a trend towards increased levels in MI/iAL and decreased levels in MI animals compared to Ctrl (Figure 1F).

### Incidence of VT/VF in MI/iAL

Because hearts of MI/iAL animals exhibited widespread deposition of interstitial fibrosis, and a pro-fibrotic molecular signature, we hypothesized that they were prone to arrhythmias, particularly during the ionic stress of hypokalemia, which was shown by Bapat et al (2) to preferentially impact fibrotic hearts. To address this, arterially-perfused porcine wedge preparations from Ctrl, MI, and MI/iAL animals were subjected to a wide range of pacing rates under conditions of normokalemia and hypokalemia. While none of the Ctrl preparations (n=0/7) exhibited onset of VT/VF during normokalemia or hypokalemia, 38% (n=3/8; MI vs. Ctrl: p=0.07) and 63% (n=5/8; Ctrl vs. MI/iAL: p=0.01) of MI and MI/iAL preparations, respectively were prone to VT/VF. Importantly, the majority (4/5) of VT/VF episodes in MI/iAL preparations arose during hypokalemic stress. In sharp contrast, none (0/5) of the MI hearts that underwent hypokalemia challenge were prone to arrhythmias (Figure 2 and Supplemental Table 1). These observations highlight a unique pro-arrhythmic response of MI/iAL hearts to hypokalemia.

Hypokalemia is known to promote arrhythmias in part by impairing repolarization, prolonging the action potential duration (APD), and forming afterdepolarization-mediated triggers. We measured the average endocardial, mid-myocardial, and epicardial APDs during normokalemia and hypokalemia (Supplemental Figure 1). Hypokalemia resulted in a comparable prolongation of APD across all muscle layers of all groups. Moreover, quantification of APD heterogeneity as indexed by the range and standard deviation of $APD_{80}$ values across the transmural wall did not reveal significant differences between groups, neither during normokalemia nor hypokalemia (Supplemental Figure 1). As such, these data discount a major role for APD prolongation or repolarization heterogeneity in the hypokalemia-mediated arrhythmias that were unique to the MI/iAL group.

Instead, we uncovered an unexpected effect on excitability in MI/iAL compared to MI and Ctrl groups (Figure 3). While an increase in pacing rate during hypokalemia resulted in the loss of 1:1 pacing capture in 86% of Ctrl and 80% of MI wedges, the same challenge resulted in loss-of-capture of only 29% of preparations from MI/iAL animals (Figure 3B), which instead were prone to pacing-induced VT/VF (Figure 2). These data highlight an intrinsically unique response of MI/iAL wedges to conditions that lower excitability, namely the combination of hypokalemia and rapid pacing.

### Rate-dependent conduction in MI/iAL

We next hypothesized that conduction abnormalities may be mechanistically involved in the pathogenesis of arrhythmias in this model. To address this, we began by measuring the basal conduction velocities ($CV_b$) in Ctrl, MI, and MI/iAL preparations. Despite a trend towards reduced $CV_b$ in MI and MI/iAL preparations relative to Ctrl, differences did not reach statistical significance (Figure 4A). Since arrhythmias in this model were elicited by progressive elevation in pacing rate during challenge with hypokalemia, we compared CV values measured just before the onset of VT/VF or the loss of 1:1 capture in Ctrl, MI, and MI/iAL preparations (Figure 4B). CV measured under these conditions of low excitability was defined as the critical CV ($CV_c$) since it represented the near final measurable level before arrhythmias were initiated or the initial loss of excitability encountered. Unlike $CV_b$,

$CV_c$ was significantly (p=0.03) lower in MI/iAL compared to Ctrl preparations (Figure 4C). In contrast, MI preparations exhibited relatively preserved (p=0.38) $CV_c$ compared to Ctrl hearts (Figure 4C). Of note, preparations that were prone to hypokalemia-mediated VT/VF were associated with a very narrow distribution of $CV_c$ values that clustered at ~13 cm/sec (Figure 5). In sharp contrast, a much wider distribution of $CV_c$ values ranging from 15 to 35 cm/sec was evident in arrhythmia-free or VT/VF (−) preparations (Figure 5).

We next examined the rate-dependent kinetics of CV in Ctrl and MI/iAL preparations during hypokalemia. To determine CV at very fast rates in Ctrl hearts, 1:1 pacing capture could be reestablished by increasing the pacing voltage once the initial loss-of-capture occurred. As shown in Figure 6A–C, we found major differences in the normalized CV restitution curves between Ctrl and MI/iAL preparations during hypokalemia. In particular, while Ctrl hearts exhibited a shallow slope of the CV restitution curves at PCL<250 ms, MI/iAL preparations were associated with a significantly steeper slope indicating a progressively decreasing CV profile over these rates. A linear fit of the normalized CV vs cycle length relationship over the relevant rates that precipitated VT/VF (PCL<250 ms), revealed a significantly (p<0.05) greater negative slope in MI/iAL compared to Ctrl (Figure 6B).

Conduction slowing is an established mechanism that promotes reentrant arrhythmias (5,11). Optical imaging in MI/iAL preparations revealed areas of functional conduction block and circuits of reentrant excitation underlying hypokalemia-mediated VT/VF (Video 1). A biophysical requirement for reentrant excitation to persist entails a short cardiac wavelength ($\lambda$) that must be smaller than the pathlength of the circuit. We measured $\lambda$ (product of APD and CV) under conditions of impaired excitability that led to VT/VF ($\lambda_c$). As shown in Figure 7A&B, $\lambda_c$ was significantly shorter in MI/iAL compared to Ctrl hearts reaching levels smaller than the physical dimensions of the wedge preparation (Figure 7A). Of note, $\lambda_c$ in the majority (5/7) of MI/iAL but not Ctrl (1/7) preparations was <2.0 cm, consistent with increased vulnerability to reentrant arrhythmias (Figure 7B).

## Discussion

In the present study, we demonstrate that a chronically elevated afterload in the setting of post-MI remodeling is associated with a major rise in interstitial fibrosis and a pro-fibrotic program (Figure 1). These structural abnormalities are associated with increased LV stiffness (not shown) and a vulnerable electrophysiological substrate that is unmasked by hypokalemia (Figure 2).

Specifically, we found that the mode of arrhythmia initiation was invariably related to conditions that reduced excitability (Figures 2 & 3). Indeed, the majority of arrhythmias were encountered during rapid pacing under hypokalemic conditions. This finding may be of clinical relevance considering the common use of diuretics in patients with chronic MI and arterial hypertension. Of note, 10–40% of patients treated with diuretics exhibit hypokalemia along with its pathological manifestations (16). Furthermore, diuretics increase the risk of SCD in patients with HF and arterial hypertension (17,18).

Our model of chronic MI/iAL allowed us to examine the mechanism underlying hypokalemia-mediated arrhythmias in the setting of increased afterload. While hypokalemia promotes a host of electrophysiological instabilities that render the heart more vulnerable to arrhythmias, including APD prolongation and enhanced automaticity (19), the mechanism underlying its pronounced effect in diseased compared to normal hearts is unclear. Our present findings highlight the importance of hypokalemia-related conduction slowing rather than repolarization instability in arrhythmias in a pre-clinical model of advanced structural heart disease. Of note, our experimental measurements of $CV_c$ (averaging 23 cm/sec) in preparations from Ctrl animals, which reflect the near minimum CV that is supported by normal cardiac tissue before loss-of-capture emerges, were consistent with the minimal attainable CV computed by Shaw and Rudy before onset of conduction failure (17 cm/s) in their *in silico* linear fiber model of normal guinea pig myocytes (20,21).

Our experimental protocol permitted the evaluation of CV levels even after the initial loss of 1:1 capture in arrhythmia-free preparations, since reliable pacing could be re-established by increasing the stimulus voltage. A major unexpected finding was that CV had already reached a near “minimal” level once the initial loss-of-capture occurred. Further increase in pacing rate did not significantly decrease CV thereafter. The unique rate-dependent kinetics of CV that we report in Ctrl preparations during conditions of low excitability (rapid pacing and hypokalemia) are marked by a flat slope of the steady-state CV restitution curve at PCL<250 ms (Figure 6). This unexpected finding is consistent with the notion that the minimal CV in these preparations failed to reach critically-slow levels that promote arrhythmias. In sharp contrast, MI/iAL wedges exhibited a markedly lower incidence of loss-of-capture and a steeper slope of rate-dependent CV slowing during hypokalemia challenge. This, in turn, resulted in a progressive decrease in CV that likely culminated in the initiation and maintenance of reentrant activation.

Another finding which prompted us to investigate the arrhythmic phenotype of MI/iAL animals was the widespread proliferation of diffuse interstitial fibrosis and the increased expression of multiple fibrosis markers (Figure 1). While fibrosis in this model did not cause conduction slowing under basal conditions, it likely facilitated the successful propagation of critically slow wavefronts under conditions of low excitability (hypokalemia and rapid pacing) that failed to generate propagating wavefronts in Ctrl and MI tissues. Of note, Rudy and colleagues elegantly demonstrated using computational modeling the concept of the “safety factor” (SF) of conduction, a dimensionless parameter that reflects the margin of safety with which the action potential propagates relative to the minimum requirements for sustained conduction. In particular, they showed that SF is increased when the loss of non-excitatory current to electrotonic interactions is diminished. Our present findings in this clinically-relevant animal model of MI/iAL provide experimental credence to these theoretical predictions, and extend them to situations in which conduction is adversely impacted by a profibrotic program that increases extracellular resistivity as opposed to Cx43 downregulation (20,21).

To further explore if differences in the rate-dependence of CV slowing during hypokalemia promoted the incidence of VT/VF in MI/iAL, we calculated $\lambda$ at baseline and during conditions leading up to the initiation of VT/VF. At baseline, arterially-perfused wedges

from Ctrl and MI/iAL animals exhibited comparable λ (not shown). In contrast, hypokalemia and rapid pacing caused a more pronounced shortening of λ in MI/iAL compared to Ctrl preparations (Figure 7), likely explaining their propensity for reentrant excitation (Supplemental Video).

## Clinical implications

In our study, VT/VF was induced by rapid pacing using frequencies that are commonly applied during anti-tachycardia pacing (ATP) therapy in clinical practice. ATP is implemented to reduce the frequency of high-energy shocks and therefore to improve the quality of life of ICD patients (22). However, this therapy carries the risk of VT initiation and/or acceleration and may increase mortality in patients (22). Indeed, our present findings provide a mechanistic framework that explains the pro-arrhythmic effects of ATP in patients with increased afterload. In addition, rapid ventricular pacing is also implemented in the context of the Transcatheter Aortic Valve Implantation (TAVI) procedure (23). In a patient population with increased afterload, a history of MI, and systolic dysfunction, rapid pacing during TAVI may promote the incidence of intraoperative VT/VF (23). Together, our present findings emphasize the need to closely monitor serum $K^+$ levels in hypertensive patients. While hypokalemia lowers diastolic excitability, hyperkalemia or treatment of MI/iAL patients with Na-channel blockers may carry a comparable risk by also impairing excitability.

## Limitations

Our *ex vivo* approach for evaluating arrhythmia susceptibility was based on challenge of preparations with rapid pacing. Indeed, the rapid rates that elicited hypokalemia-mediated VT/VF in the wedge preparation do not reflect the typical average heart rates in patients. Having said that, our proposed mechanism for arrhythmia initiation in this model which is based on the shortening of the cardiac wavelength below the pathlength of a reentrant circuit is likely to be underestimated in the porcine wedge preparation owing to its small dimensions (~3×1.5×1.5 cm) relative to that of the intact heart. As such, pacing-induced arrhythmias in the intact failing heart are expected to be encountered at slower rates than the ones we report in our wedge preparations. Moreover, closely-coupled premature ventricular contractions which are frequently observed in failing hearts especially during hypokalemia are likely to be associated with similar conduction patterns and arrhythmia risk as shown here for rapid pacing. This challenge, however, was not directly tested in our studies.

Another key limitation is the absence of adrenergic signaling in our *ex vivo* perfused preparations. Of note, Lang et al. (14) demonstrated in their arterially perfused wedge preparations from failing human hearts the importance of selective β2-adenoreceptor activation in the exacerbation of electrical remodeling and arrhythmias. This factor was not accounted for in our experimental design.

## Perspectives

**Competency in Medical Knowledge—**A chronically elevated afterload in the setting of post-myocardial infarction (MI) remodeling is associated with a major rise in interstitial fibrosis and a pro-fibrotic gene program. These structural abnormalities produce a

vulnerable electrophysiological substrate that is unmasked by hypokalemia. The importance of hypokalemia-related conduction slowing and reduced conduction reserve at elevated heart rates is underscored.

**Translational Outlook—**Our findings of reduced conduction reserve in this new clinically-relevant porcine highlight the need to closely monitor serum potassium levels and heart rate in ischemic heart failure patients with resistant hypertension.

## Supplementary Material

Refer to Web version on PubMed Central for supplementary material.

## Acknowledgments

**Funding:** This work was supported by grants from the National Institutes of Health (R01 HL091923 and R21AG054211) and the American Heart Association (13GRNT17000046) to FGA.

Authors wish to thank Ms. Lauren Leonardson for outstanding technical support.

## ABBREVIATIONS

| | |
|---|---|
| **CTGF** | connective tissue growth factor |
| **Ctrl** | Control group |
| **$CV_b$** | basal conduction velocity |
| **$CV_c$** | critical conduction velocity |
| **DT** | diastolic threshold |
| **EF** | ejection fraction |
| **ICD** | implantable cardiac defibrillator |
| **LCx** | left circumflex artery |
| **LV** | left ventricle |
| **MI** | myocardial infarction |
| **MI/iAL** | MI model with increased afterload |
| **TAVI** | Transcatheter Aortic Valve Implantation |
| **VTI** | velocity time integral |
| **VT/VF** | sustained ventricular tachycardia/ventricular fibrillation |
| **WGA** | wheat-germ agglutinin |
| **$\lambda$** | cardiac wavelength |
| **$\lambda_c$** | critical cardiac wavelength |

## References


1. Smith SM, Gong Y, Handberg E, et al. Predictors and outcomes of resistant hypertension among patients with coronary artery disease and hypertension. Journal of hypertension. 2014; 32:635–43. [PubMed: 24299915]
2. Bapat A, Nguyen TP, Lee JH, et al. Enhanced sensitivity of aged fibrotic hearts to angiotensin II- and hypokalemia-induced early afterdepolarization-mediated ventricular arrhythmias. Am J Physiol Heart Circ Physiol. 2012; 302:H2331–40. [PubMed: 22467308]
3. Akar FG, Nass RD, Hahn S, et al. Dynamic changes in conduction velocity and gap junction properties during development of pacing-induced heart failure. Am J Physiol Heart Circ Physiol. 2007; 293:H1223–30. [PubMed: 17434978]
4. Akar FG, Rosenbaum DS. Transmural electrophysiological heterogeneities underlying arrhythmogenesis in heart failure. Circ Res. 2003; 93:638–45. [PubMed: 12933704]
5. Akar FG, Spragg DD, Tunin RS, Kass DA, Tomaselli GF. Mechanisms underlying conduction slowing and arrhythmogenesis in nonischemic dilated cardiomyopathy. Circ Res. 2004; 95:717–25. [PubMed: 15345654]
6. Akar FG, Tomaselli GF. Conduction abnormalities in nonischemic dilated cardiomyopathy: basic mechanisms and arrhythmic consequences. Trends Cardiovasc Med. 2005; 15:259–64. [PubMed: 16226681]
7. Akar FG, Yan GX, Antzelevitch C, Rosenbaum DS. Unique topographical distribution of M cells underlies reentrant mechanism of torsade de pointes in the long-T syndrome. Circulation. 2002; 105:1247–53. [PubMed: 11889021]
8. Ishikawa K, Ladage D, Tilemann L, Fish K, Kawase Y, Hajjar RJ. Gene transfer for ischemic heart failure in a preclinical model. J Vis Exp. 2011
9. Ishikawa K, Aguero J, Oh JG, et al. Increased stiffness is the major early abnormality in a pig model of severe aortic stenosis and predisposes to congestive heart failure in the absence of systolic dysfunction. Journal of the American Heart Association. 2015:4.
10. Boukens BJ, Sulkin MS, Gloschat CR, Ng FS, Vigmond EJ, Efimov IR. Transmural APD gradient synchronizes repolarization in the human left ventricular wall. Cardiovasc Res. 2015; 108:188–96. [PubMed: 26209251]
11. Glukhov AV, Fedorov VV, Kalish PW, et al. Conduction remodeling in human end-stage nonischemic left ventricular cardiomyopathy. Circulation. 2012; 125:1835–47. [PubMed: 22412072]
12. Glukhov AV, Fedorov VV, Lou Q, et al. Transmural dispersion of repolarization in failing and nonfailing human ventricle. Circ Res. 2010; 106:981–91. [PubMed: 20093630]
13. Holzem KM, Gomez JF, Glukhov AV, et al. Reduced response to I blockade and altered hERG1a/1b stoichiometry in human heart failure. J Mol Cell Cardiol. 2015
14. Lang D, Holzem K, Kang C, et al. Arrhythmogenic remodeling of beta2 versus beta1 adrenergic signaling in the human failing heart. Circ Arrhythm Electrophysiol. 2015; 8:409–19. [PubMed: 25673629]
15. Lou Q, Fedorov VV, Glukhov AV, Moazami N, Fast VG, Efimov IR. Transmural heterogeneity and remodeling of ventricular excitation-contraction coupling in human heart failure. Circulation. 2011; 123:1881–90. [PubMed: 21502574]
16. Gennari FJ. Hypokalemia. N Engl J Med. 1998; 339:451–8. [PubMed: 9700180]
17. Cooper HA, Dries DL, Davis CE, Shen YL, Domanski MJ. Diuretics and risk of arrhythmic death in patients with left ventricular dysfunction. Circulation. 1999; 100:1311–5. [PubMed: 10491376]
18. Siscovick DS, Raghunathan TE, Psaty BM, et al. Diuretic therapy for hypertension and the risk of primary cardiac arrest. N Engl J Med. 1994; 330:1852–7. [PubMed: 8196728]
19. Pezhouman A, Singh N, Song Z, et al. Molecular Basis of Hypokalemia-Induced Ventricular Fibrillation. Circulation. 2015
20. Shaw RM, Rudy Y. Ionic mechanisms of propagation in cardiac tissue. Roles of the sodium and L-type calcium currents during reduced excitability and decreased gap junction coupling. Circ Res. 1997; 81:727–41. [PubMed: 9351447]

21. Wang Y, Rudy Y. Action potential propagation in inhomogeneous cardiac tissue: safety factor considerations and ionic mechanism. Am J Physiol Heart Circ Physiol. 2000; 278:H1019–29. [PubMed: 10749693]

22. Moss AJ, Schuger C, Beck CA, et al. Reduction in inappropriate therapy and mortality through ICD programming. N Engl J Med. 2012; 367:2275–83. [PubMed: 23131066]

23. Masson JB, Kovac J, Schuler G, et al. Transcatheter aortic valve implantation: review of the nature, management, and avoidance of procedural complications. JACC Cardiovasc Interv. 2009; 2:811–20. [PubMed: 19778768]

## HIGHLIGHTS

- Although the pathophysiological significance of hypertension in post-MI patients is established, mechanisms by which increased afterload alters the electrophysiological substrate and promotes arrhythmias following MI is unknown.
- We developed a new porcine model of post-MI remodeling with chronically increased afterload (MI/iAL) that exhibits widespread interstitial fibrosis, increased profibrotic gene expression, and propensity to pacing-induced arrhythmias when challenged with hypokalemia.
- Investigation of the electrophysiological substrate revealed the dependence of these arrhythmias on hypokalemia-mediated conduction and not repolarization abnormalities.
- A steep negative slope of rate-dependent conduction slowing in MI/iAL is consistent with a high safety factor for propagation of slow wavefronts before onset of VT/VF.
- Fibrosis in MI/iAL promotes the successful propagation of critically slow wavefronts leading to reentrant arrhythmias that are unmasked by hypokalemia.

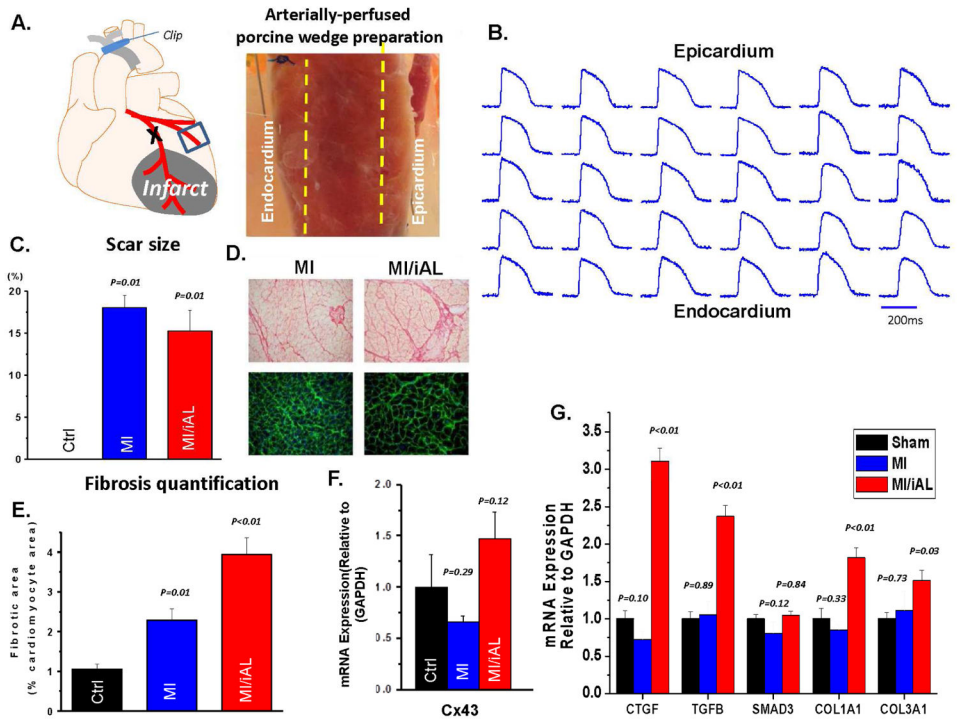


**Figure 1.**

**A.** Schematic representation and image of the arterially-perfused porcine wedge preparation. **B.** Representative transmural optical action potentials measured from across the ventricular wall of the wedge preparation. **C.** Quantification of scar size using triphenyl-tetrazolium chloride staining. **D.** Images of picro-sirius red (fibrosis; above) and WGA (hypertrophy; bottom) staining showing advanced structural remodeling in MI/iAL hearts. **E.** Bar graphs show quantitation of interstitial collagenous tissue area against the cardiomyocyte area showing pronounced fibrotic remodeling in MI/iAL. **F.** Cx43 mRNA expression in Ctrl, MI/iAL and MI animals was not different. **G.** Quantitation of fibrosis related gene expression at the mRNA level. CTGF, TGF-β, COL1A1, and COL3A1 but not SMAD3 are markedly upregulated in MI/iAL compared to MI and Ctrl hearts. 3 pig hearts for each group were used for RT-PCR analyses.

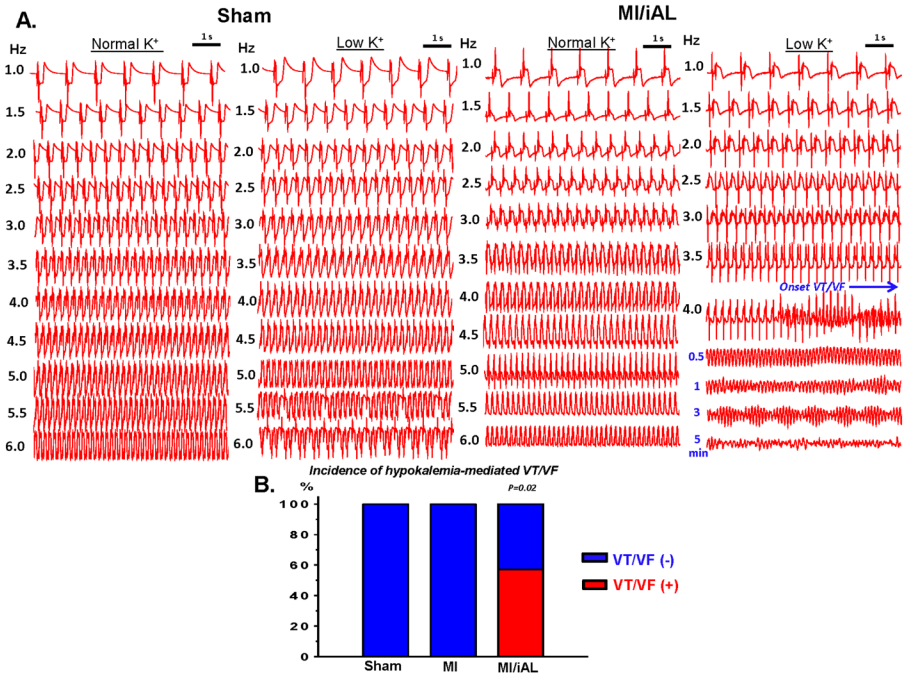


**Figure 2.**

**A.** Representative electrogram recordings from Ctrl and MI/iAL preparations during normokalemia and hypokalemia. Arterially-perfused wedges from MI/iAL but not Ctrl animals were prone to VT/VF during challenge with rapid pacing under conditions of hypokalemia. **B.** Incidence of VT/VF in Ctrl (n=7), MI (n=5), and MI/iAL (n=7) during hypokalemia.

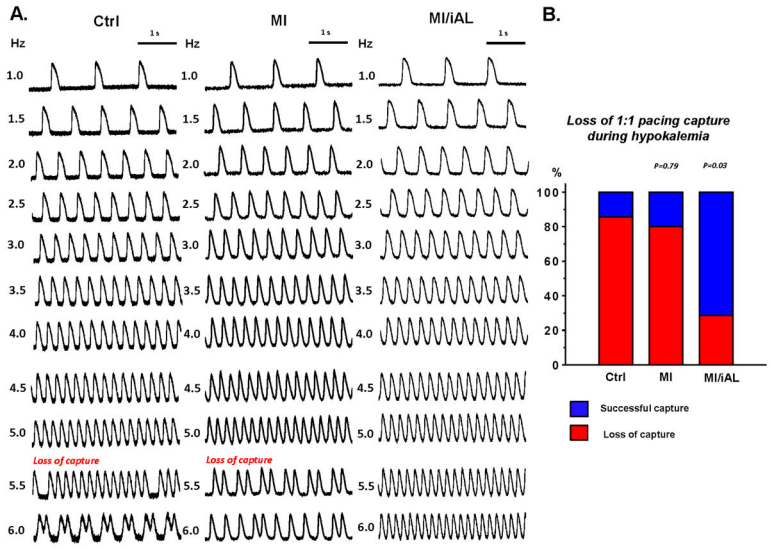


**Figure 3.**

Loss of 1:1 pacing capture during hypokalemia: **A.** Representative optical action potentials recorded at progressively faster pacing rates (1.0–6.0 Hz) from Ctrl, MI and MI/iAL wedges during hypokalemia. **B.** Incidence of pacing-induced loss of 1:1 capture in Ctrl (n=7), MI (n=5) and MI/iAL (n=7) preparations.

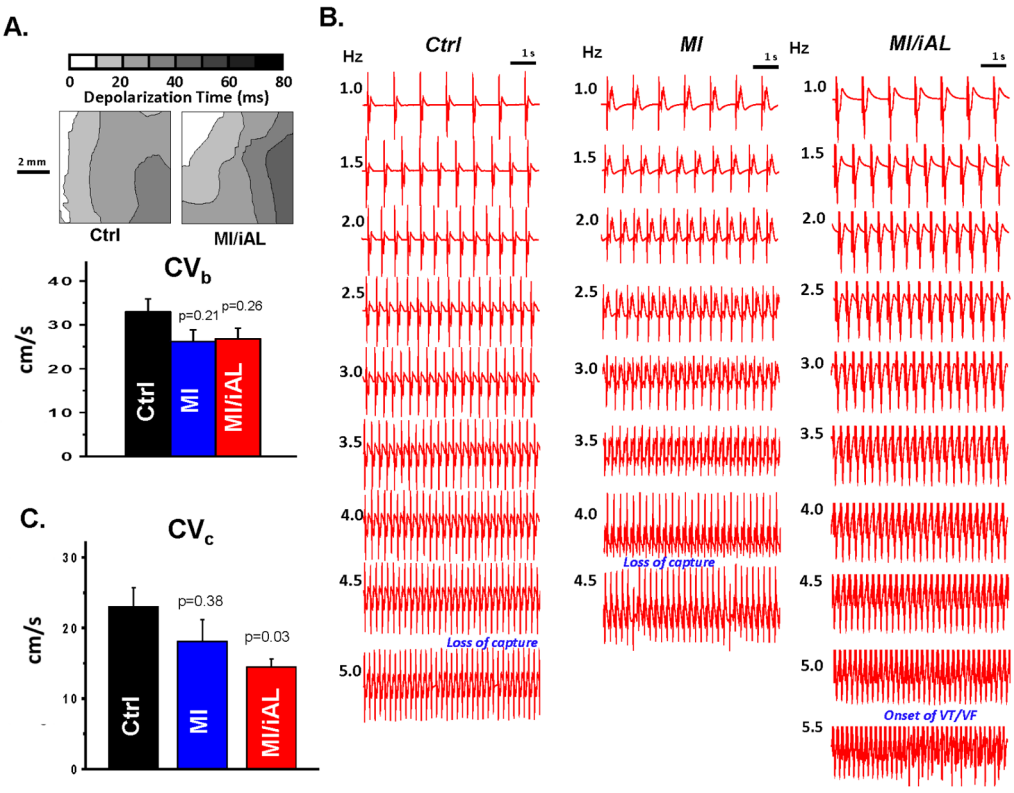


**Figure 4.**

**A.** Representative depolarization isochrone maps from Ctrl and MI/iAL preparations at baseline (Normokalemia, PCL 1000ms). Comparison of $CV_b$ in Ctrl, MI, and MI/iAL preparations (Ctrl: n=11, MI: n=9 and MI/iAL: n=10). No significant differences in $CV_b$ were found between MI or MI/iAL compared to Ctrl preparations. **B.** Representative electrogram traces recorded at a wide range of pacing rates in Ctrl, MI, and MI/iAL preparations during hypokalemia challenge. **C.** Comparison of average $CV_c$ (Ctrl: n=7, MI: n=4 and MI/iAL: n=7) indicating significantly decreased levels in the MI/iAL group.

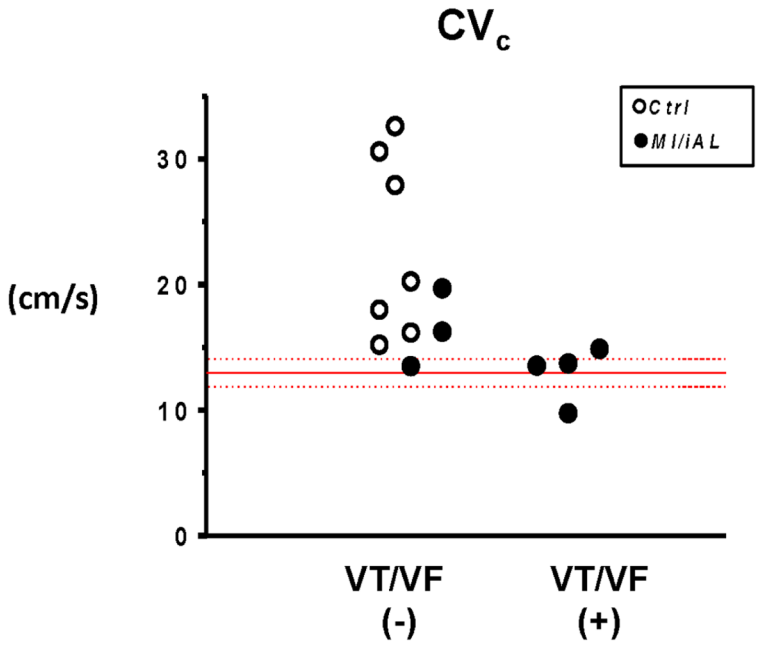


**Figure 5.**

Individual values of $CV_c$ for VT/VF (+) versus VT/VF (−) preparations. VT/VF (+): preparations that exhibited sustained VT/VF, VT/VF (−): preparations that did not exhibit VT/VF. $CV_c$: critical CV.

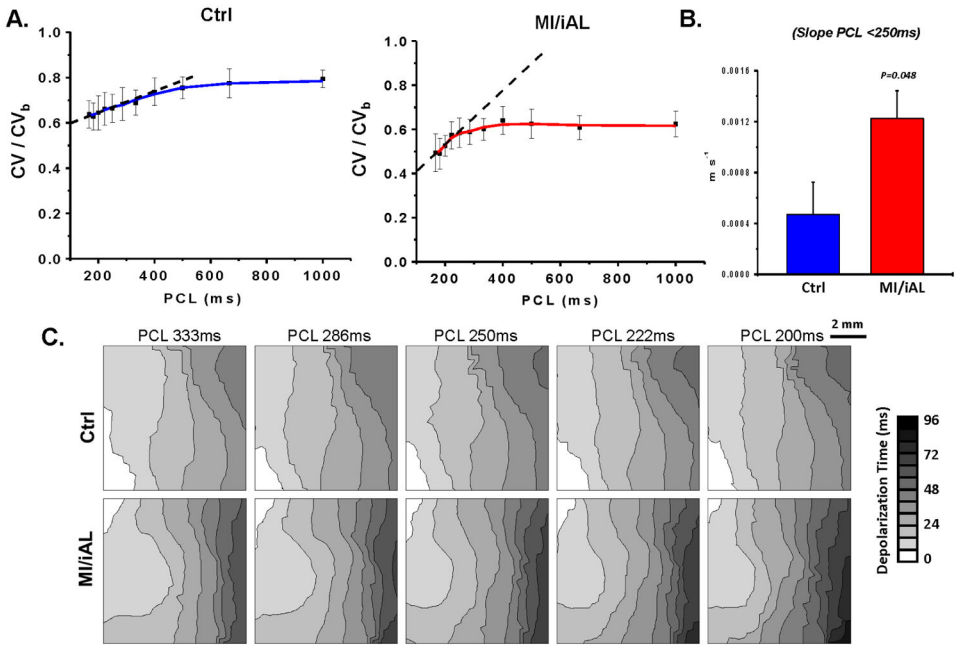


**Figure 6.**

**A.** Rate dependent conduction slowing during hypokalemia in wedges from Ctrl (n=6) and MI/iAL (n=5) animals. CV at each rate is normalized to $CV_b$. **B.** Corresponding average linear slope of normalized CV restitution curves in Ctrl and MI/iAL wedges during hypokalemia at PCL<250 ms. **C.** Representative depolarization isochrone maps from Ctrl and MI/iAL wedges.

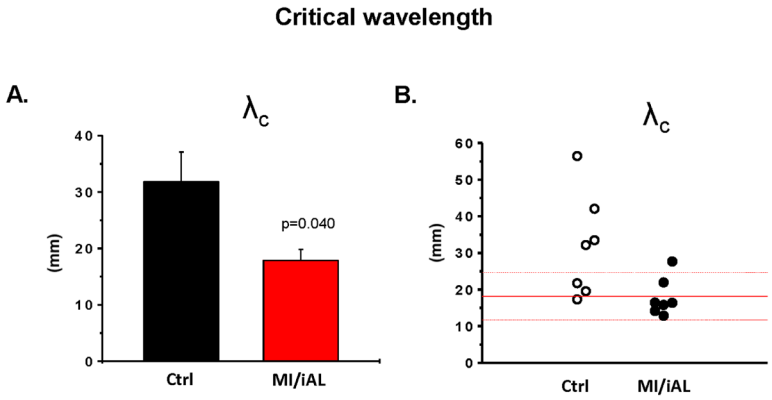


**Figure 7.**

**A**. The critical cardiac wavelength ($\lambda_c$) in Ctrl (n=7) and MI/iAL (n=7) wedges. $\lambda_c$ was defined as the cardiac wavelength during hypokalemia at the fastest pacing rate before initiation of VT/VF, loss of 1:1 capture or at the end of the protocol if neither occurred. **B.** Individual values of $\lambda_c$.

**Table 1**

Primers

| Gene name | Forward primer (5′-3′) | Reverse primer (5′-3′) |
|---|---|---|
| GAPDH | CAATGACCCCTTCATTGACC | GAAGATGGTGATGGCCTTTC |
| CTGF | GTGCACAGCCAAAGATTGTG | TGGTATTTGCAGCTGCTCTG |
| TGFB | AAAACAGGAAGGCAGTGTGG | TAGGCTGCTTTCTTGGCTTC |
| SMAD3 | TTCTCCCTCAACCAAAGTGG | GAGCAGAAGCCATTTCTTGC |
| COL1A1 | TTCTGCAACATGGAGACAGG | TCTTGTCCTTGGGGTTCTTG |
| COL3A1 | TCCTCCTGGAAAGAATGGTG | TCCAGGCAAGCCTTGTAATC |
| Cx43 | TCATGCTGGTCGTATCCTTG | TCTTTCCCTTCACACGATCC |